Modeling of Airfoil Trailing Edge Flap with Immersed Boundary Method

Zhu, Wei Jun; Shen, Wen Zhong; Sørensen, Jens Nørkær

Published in:
ICOWEOE-2011

Publication date:
2011

Document Version
Publisher's PDF, also known as Version of record

ICOWEOE-2011-07

MODELING OF AIRFOIL TRAILING EDGE FLAP WITH IMMERSED BOUNDARY METHOD

Wei Jun Zhu, Wen Zhong Shen and Jens Nørkær Sørensen

Department of Mechanical Engineering, Technical University of Denmark,
DK-2800 Lyngby, Denmark

Abstract

The present work considers incompressible flow over a 2D airfoil with a deformable trailing edge. The aerodynamic characteristics of an airfoil with a trailing edge flap is numerically investigated using computational fluid dynamics. A novel hybrid immersed boundary (IB) technique is applied to simulate the moving part of the trailing edge. Over the main fixed part of the airfoil the Navier-Stokes (NS) equations are solved using a standard body-fitted finite volume technique whereas the moving trailing edge flap is simulated with the immersed boundary method on a curvilinear mesh. The obtained results show that the hybrid approach is an efficient and accurate method for solving turbulent flows past airfoils with a trailing edge flap and flow control using trailing edge flap is an efficient way to regulate the aerodynamic loading on airfoils.

Nomenclature

A	amplitude
C_l	lift coefficient
f	frequency
f_i	volume force
k	kinetic energy / frequency
v_i	forcing cell velocity
U_i	flow velocity components
P	pressure
t	time
x_i	coordinates
α	angle of attack / pitch angle
β	trailing edge angle
ν	kinematic viscosity
ν_t	eddy viscosity
ω	specific dissipation rate
ρ	density

Acronyms

CFD	computational fluid dynamics
IB	immersed boundary
LES	large eddy simulation
NS	Navier-Stokes
RANS	Reynolds averaged Navier-Stokes
RHS	right hand side

Introduction

The IB method has been developed to handle flows over complex wall geometries or moving geometries. The immersed boundary method is ideally designed for Cartesian grid solvers [1, 2]. The wall surface is represented with forcing terms which are added as additional terms in the NS equations. The significant advantage of using such technique is the great simplification of grid regeneration around the moving objects. The IB method provides an alternative numerical method to solve complex flow problems, such as flow over airfoil with deformable trailing edge. By combining the IB model into the existing in-house flow solver, it is expected that the detailed flow field around a deformable trailing edge can be achieved with standard computational effort. Such a numerical tool will also have potential value for different applications other than modeling airfoil flow problems.

The IB method is namely that the solid boundaries are immersed on grids that normally don't conform to the shape. Ideally, the IB approach requires only simple Cartesian grid

instead of body conformal grid. For numerical simulations, the required input data is the prescribed IB surface shape. To simulate different body geometries, the only change is the IB surface data and the computational mesh is not modified. In other words, the IB surface movement has to be prescribed as preprocessing. For a given IB surface, the grid does rarely conform to the IB surface. In case that the IB surface cuts through the grid lines, the IB surface would be represented by the neighboring grid points. Therefore the issue of imposing wall boundary conditions at IB surface is the key factor. This would require modifying the NS equations in the vicinity of the IB surface. Detailed discussions of wall treatment are presented in the following sections in this paper.

To apply the IB technique in turbulent flow conditions, the particular challenge is to model the wall turbulence boundary layer at high Reynolds numbers. It turns out that the wall model both affects the accuracy of the solver and the solution convergence. Kalitzin and Iaccarino [3, 4] applied one equation [5] and two equations [3] turbulence models together with the IB method. The turbulence models have zero wall boundary conditions for all turbulence variables. They proposed look-up tables to model turbulence variables such as eddy viscosity. LES model is the other option of turbulence modeling. Tessicini et al. [6] modeled a hydrofoil trailing edge flow using the IB method in conjunction with LES where a near-wall model is investigated. In Eisenbach and Friedrich [7], airfoil flow at high angle of attack is simulated in the framework of IB method for LES where they introduced the block cell interface concept. Comparing the RANS and LES turbulence models, the LES model is more straightforward to be used since it does not require any wall functions but only sensitive to mesh density. The RANS turbulence model produces averaged flow solutions which is more feasible for the present study. From the control point of view, the LES turbulence model will give much difficulty since all flow quantities are fluctuating around the mean value. Here we proposed a hybrid method that combines wall-bounded flow solver together with IB technique. In this manner, only the moving part of the solid body is modeled by IB method. This ensures much better accuracy at the static part of solid body and also enhanced the mesh density at the moving part.

The paper is organized as following: section 2 introduces the governing equations that combined with the IB technology; section 3 presents the classical result of laminar flow over a cylinder using both standard CFD in curvilinear mesh and the IB method in a Cartesian grid system; section 4 focuses on turbulent flow over a NACA 0012 airfoil with a combined motion of pitch and trailing edge flap; section 5 shows an active control case using trailing edge flap. A conclusion in given in the final section.

Numerical method

The present version of the IB technique is based on the Reynolds-averaged incompressible NS equations and the continuity equation,

$$\frac{\partial U_i}{\partial t} + \frac{\partial (U_i U_j)}{\partial x_j} = -\frac{1}{\rho}\frac{\partial (P + 2/3\rho k)}{\partial x_i} + \frac{\partial}{\partial x_j}\left[(\nu + \nu_t)\left(\frac{\partial U_i}{\partial x_j} + \frac{\partial U_j}{\partial x_i}\right)\right] + f_i \qquad (1)$$

$$\frac{\partial U_i}{\partial x_i} = 0$$

where the body force f_i creates the desired velocity field along the solid boundary; P is the pressure, ρ is the density of air, and U_j denotes the velocity components. ν is the kinematic viscosity, ν_t is the turbulent eddy viscosity and k is the turbulent kinetic energy,

obtained from the turbulence model. In the IB method, the forcing term f_i is determined from a time discretization of Equation (1),

$$\frac{U_i^{n+1} - U_i^n}{\Delta t} = RHS^{n+1/2} + f_i^{n+1/2} \qquad (2)$$

where the RHS results from the discretization of the convective, viscous and pressure-gradient terms at time level $n+1/2$. The notation of f_i at $n+1/2$ means direct forcing, i.e. the forcing term is being computed before the velocity but at the same time step. From Equation (2), the volume force f_i which yields the desired velocity v^{n+1} simply is written as [2, 8, 9]

$$f_i^{n+1/2} = -RHS^{n+1/2} + \frac{v_i^{n+1} - U_i^n}{\Delta t}. \qquad (3)$$

Solving the flow equation with the forcing terms determines the velocity on the wall represented by the IB. The velocity v_i^{n+1} on the forcing cells is determined by linear interpolation between the wall surface and the neighbouring grid points.

In the present work, the IB methodology is adapted to the k–ω turbulence model of Menter [10]. To employ the k–ω model in the framework of the IB method, the wall normal distance to the IB surface y_{ib} is introduced such that

$$y = \min(y, y_{ib}). \qquad (4)$$

Therefore, the wall distance function is determined either from the solid wall or from the IB surface. Thus, the near wall boundary conditions on IB cells are given as

$$k_w = 0$$
$$\omega_{ib} = \frac{60}{\rho \cdot \beta \cdot (\Delta y_{ib})^2} \qquad (5)$$

To satisfy the boundary conditions of the turbulent quantities, the turbulent kinetic energy, k, is set to zero inside the body and on the IB surface. The ω-values on the IB surface are calculated using the local normal distance from the forcing cells to their nearest IB surface. For stability reasons, the ω values inside the body can not be attributed a constant value, as it creates a discontinuity when going from the solid body to the flow region. A practical way to circumvent this problem is to apply Equations (4) and (5) also inside the solid body. This ensures a smooth distribution of ω-values everywhere in the computational domain. In the case of a moving body, the distance y_{ib} needs to be re-calculated at each time-step and compared with the distance from solid walls.

To locate the cells that define the immersed boundary, the method of ray tracing is applied. This is illustrated in Figure 1, which depicts the IB surface, the body cells and the outside cells around a solid body. Applying ray tracing to determine the location of points A and B, it is observed that the ray starting from point A has crossed the IB surface two times, whereas the one starting at point B has three cross points. The general rule is that a point is located outside the solid body if the ray emanating from it has zero or an even number of cross points with the IB surface.

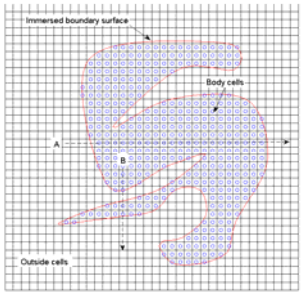

Figure 1. Location of body cells (open circles) using ray tracing method.

Laminar flow over a cylinder

As the IB method is initially designed for low Reynolds number flows with Cartesian grid, we start with laminar flow over cylinder as the first test case. The flow Reynolds number is set at 100. In this case, the equal spacing Cartesian mesh is used such as shown in Figure 2. The solid boundary is represented by the solid line which is immersed in the grid. Knowing all the cells cut though the IB line, the cylinder geometry is finally represented by the cell center points near the IB line as shown in Figure 2.

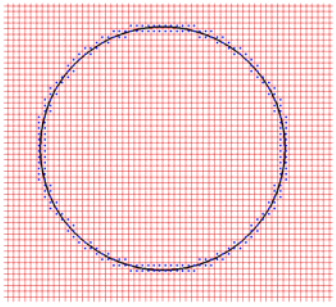

Figure 2. Cartesian mesh for IB simulation.

To compare the quality of IB technique, the same flow is performed by standard curvilinear mesh. Figure 3 shows the flow vorticity of two methods at same time instant. As it is seen, the two simulations yield similar flow field. Although very coarse grid is applied, the present IB simulation still provides good accuracy. The more detailed comparison is given in Figure 4 where the pressure coefficients of the two simulations are compared. There is good general agreement with two methods. The solution can be further improved if finer mesh is introduced.

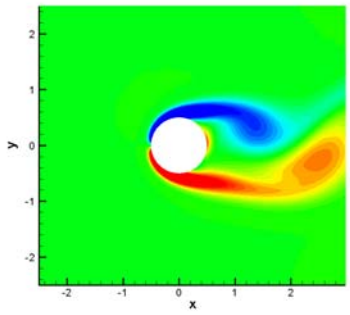

(a)

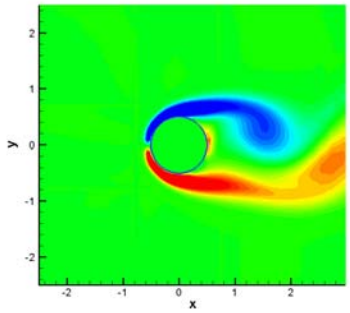

(b)

Figure 3. Curvilinear (a) and IB (b) simulations.

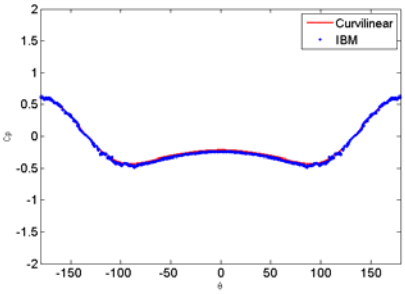

Figure 4. Comparison of the Cp distribution along the cylinder surface.

Complex turbulent flow case

In this section, turbulent flow past an airfoil that combines pitching and trailing edge flapping is considered. Previous experimental investigations [11] showed that this motion is associated with a complex flow behaviour due to the phase lag between the pitch and flap angles. In such a case, the unsteady aerodynamic load is dependent on the combination of the pitch and flap

angles. In the following the IB method will be validated for this combined motion by comparing numerical simulations with experimental results [11].

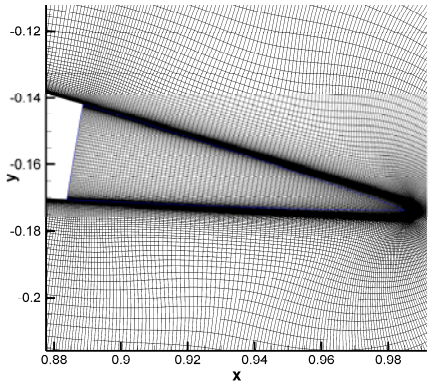

Figure 5. Mesh near the trailing edge part.

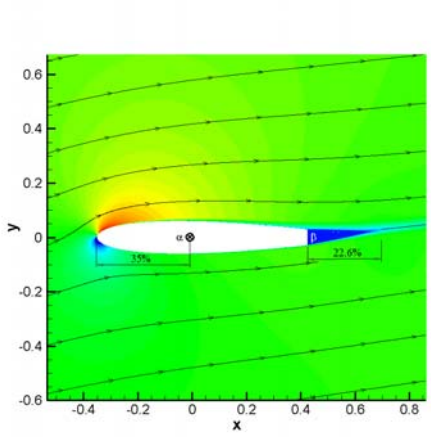

Figure 6. Sketch of airfoil subject to combined pitching and flapping movement with instantaneous plots of stream-wise velocity contours and stream-lines.

The airfoil under study is the NACA 0012 and the mesh configuration is shown in Figure 5. The trailing edge flap is 22.6% percent of the airfoil chord length. The grid lines are clustered along the virtual trailing edge which is now represented by IB. In order to utilize a similar setup as in the experiment, the numerical trailing edge flap has rigid movement as well. It should be noted that long trailing edge flaps mainly are aimed for high lift devices, such as wings of aircraft. However, it is still a good reference for wind turbine blade applications. The airfoil pitching axis is located at a chord wise position of 35% percent of the airfoil chord measured from the leading edge, as depicted in Figure 6. In the figure, the pitch and flap angles are referred to as α and β, respectively. The airfoil movement is given as $\alpha(t) = \alpha_0 + A\sin(2k_1 t)$ and $\beta(t) = \beta_0 + B\sin(2k_2 t - \phi)$, where ϕ denotes the phase shift between the two oscillations. The airfoil is pitching at a mean angle $\alpha_0=4^\circ$, an amplitude $A=6^\circ$, and a reduced frequency k_1=0.021. The flap has a similar motion with $\beta_0=0^\circ$, an amplitude $B=5.4^\circ$, and a reduced frequency k_2=0.042 ($k_2=2k_1$).

The flow is simulated at a Reynolds number of 1.63×10^6, with an initial angle of attack $\alpha_0=4^\circ$. A snapshot of the stream-wise velocity contours and stream lines is shown in Figure 6. Since the pitching motion of the airfoil is performed by oscillating the computational grid instead of moving the airfoil, the pitch angle is observed as a directional change of the stream lines. The results are here compared to experiments [11] at different phase lags between the flap and the airfoil pitching movements. The time history of the pitch and flap angles, and associated lift curves, are shown for $\phi=148^\circ$, 294°, and 357° in Figures (7), (8) and (9), respectively. As seen in the figures, the airfoil pitch and flap motions in the experiment do not exactly correspond to sinusoidal shapes. Due to mechanical oscillations in the model system, measurement errors exist for both pitch and flap motions. The numerical results, however, are generally in very good agreement with the experimental data, demonstrating that the IB technique has the flexibility of dealing with complex airfoil motion. The advanced numerical tool also provides a much better accuracy than the simplified tools used in [11]. The different shapes of the loops presented in

Figures (7)-(9) are due to the different phase angles between the flap and airfoil motions. For a pitching airfoil with a fixed flap, one would expect an open 'o'-like loop. By combining the flap movement with airfoil pitching, the unsteady aerodynamics becomes more complicated. The effect caused by the flap movement is similar to a simultaneously altering of the airfoil shape, corresponding e.g. to a cambering or a de-cambering of the airfoil shape. In Figure 7, at a time instant $t \approx 0.065$, the pitch and flap angles attain approximately their maximum value at the same time. This corresponds to a maximum cambering effect, and a maximum lift value is seen to occur at $\alpha_0=10^o$. A similar tendency is shown in Figure 8 at a time instant $t \approx 0.055$, where the flap angle attains its minimum value at the same time as the pitch angle attains a maximum value. Due to the maximum de-cambering effect from the flap, the maximum lift is decreased, as compared to Figure 7.

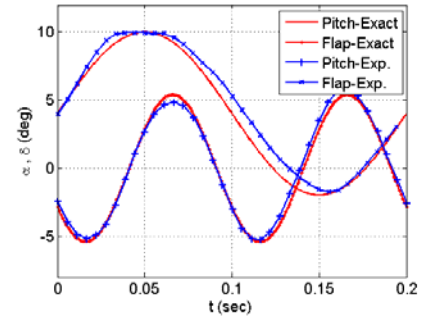

(a)

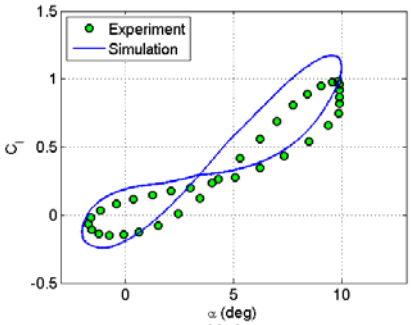

(b)

Figure 7. (a) Motion of the pitch and flap angles. (b) Comparison of the computed lift coefficient with experiment at a phase lag of 148^o.

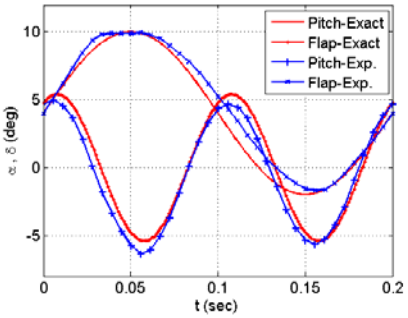

(a)

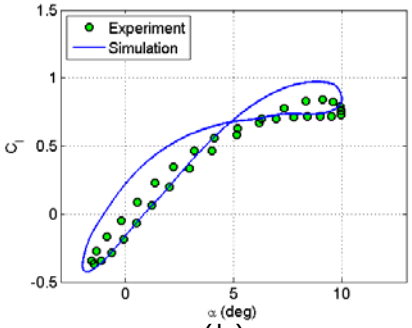

(b)

Figure 8. (a) Motion of the pitch and flap angles. (b) Comparison of the computed lift coefficient with experiment at a phase lag of 298^o.

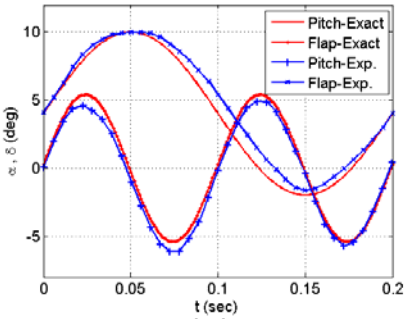

(a)

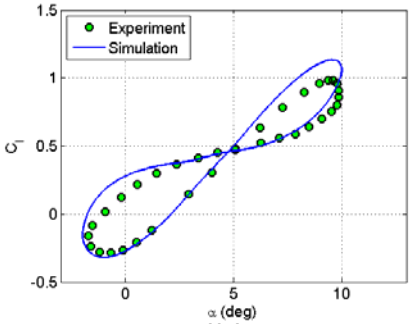

(b)

Figure 9. (a) Motion of the pitch and flap angles. (b) Comparison of

the computed lift coefficient with experiment at a phase lag of 357^o.

Flow control study

In this section we considered a flow control case using NACA 63418 airfoil with a 15%-chord adaptive trailing edge. The purpose of this study is to show the ability of using trailing flap to control the loading on a wind turbine airfoil. The numerical calculation will also give some guide lines for the similar experiments that will be carried out at DTU/MEK wind tunnel. Therefore, the simulation uses nearly the same geometric configurations as the experimental setup. Figure 10 illustrates some features of the numerical mesh configurations. The velocity at inlet is V = 10 m/s, the test section has dimension of 0.5m x 0.5m, the airfoil chord is 0.2m and the trailing edge flap is 0.03m. Two small airfoils are placed in front of the main airfoil. The small airfoils have a chord of 0.1 m and they are located at the positions of A(-0.1,0.1) and B(-0.1,-0.1), where the leading edge of the main airfoil is located at (0,0). The task of the two small airfoils above and below the main airfoil is to sinusoidally pitch the inflow and therefore change the angle of attack at the main airfoil. The two airfoils are modeled by adding two point forces in the momentum equations of NS equations

$$Lift = 0.5\sin(2\pi ft). \qquad (6)$$

By applying such a prescribed force at point A and B, the desired velocity field is obtained which yields the change of angle of attack at the main airfoil.

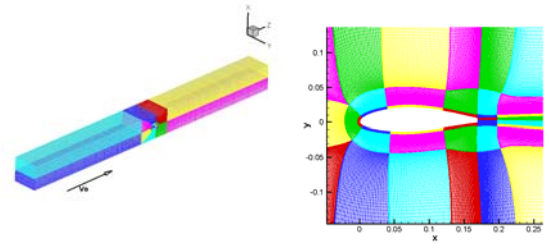

Figure 10. Mesh configureation

The flow vorticity is shown in Figure 11 where the effect at the two forcing points is observed as voticity. For flow at zero angle of attack, the steady lift is achieved at C_l = 0.18 for NACA 63418 airfoil. If we start to pitch the small airfoils and with the purpose to still maintain the steady lift at C_l = 0.18, a corresponding motion of the trailing edge flap of NACA 63418 airfoil shall be prescribed. Here, a P-controller is applied to control the flap angle, e.g., $\beta = k*(C_l - 0.18)$ where k is a constant to adjust the angular speed of the trailing edge. The lift coefficient from the main airfoil is shown in Figure 12 as function of simulation time. At the time interval of t = [0,10], the simulation was only performed for the main airfoil. It is seen that flow is quickly stabilized at C_l = 0.18. At the second time interval of t = [10, 12], the two small airfoils start to pitch in the same manner as in Equation (6) with a frequency of 1. The periodic lift curve is created as it is expected. At the third time interval t = [12, 20], the control of the trailing edge is activated by using the P-controller. It is see that for the present case, the simple P-controller is sufficient to maintain the main airfoil at a desired constant value.

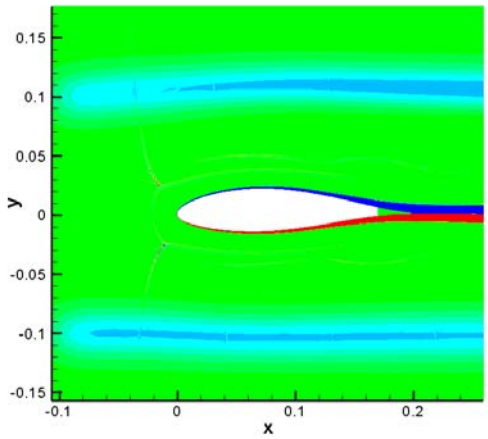

Figure 11. Vorticity contour plot with the two oscillating airfoils and the main airfoil.

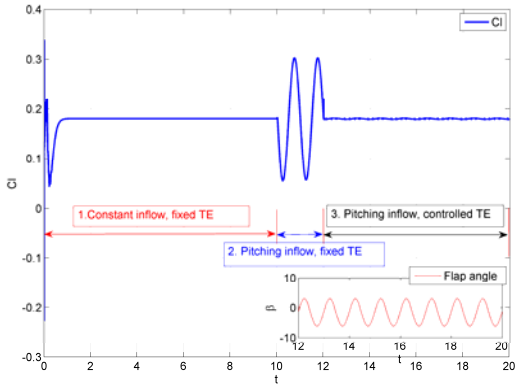

Figure 12. Time series lift coefficient at controlled and uncontrolled period.

Conclusion

The present paper described the development of a hybrid immersed boundary method. The method is developed with the aim of controlling aerodynamic loading for turbulent flows past wind turbine airfoils. The principle of the new IB method is to employ a standard CFD on a structured mesh over most of the airfoil and utilize the IB technique to model the movement of the trailing edge flap. The model is implemented into an existing incompressible Reynolds-averaged Navier-Stokes code. Special attention was paid to turbulent flows, where the IB methodology has been adapted to a k-ω turbulence model. The IB method combines the advantages of the IB technique with the efficiency of applying a standard CFD method on a structured mesh. In the case of a combined pitching and flapping motion simulations were compared to existing experiments. The time behaviour of the computed lift coefficient was in excellent agreement with measured values. The simulations clearly demonstrated the robustness and accuracy of treating complex airfoil movements by the IB formulation. Furthermore, an investigation of load control with trailing edge flap has shown great potential even with a simple control method.

Acknowledgements

The authors would like to acknowledge the Danish National Advanced Technology Foundation (Højteknologifonden) and Vestas Wind Systems A/S for supporting this research work. The numerical simulations were carried out on a cluster sponsored by the Danish Centre for Scientific Computing.

References

[1] Mittal, R., and Iaccarino, G., “Immersed Boundary Methods,” Annual Review of Fluid Mechanics, Vol. 37, 2005, pp. 239–261. doi:10.1146/annurev.fluid.37.061903.175743

[2] Mohd-Yosuf J., “Combined immersed boundary/B-spline methods for simulation of flow in complex geometries”, Annu. Res. Briefs, Cent. Turbul. Res., 1997. pp. 317–28

[3] Georgi Kalitzin and Gianluca Iaccarino, “Turbulence modeling in an immersed-boundary RANS method” , Center for Turbulence Research Annual Research Briefs 2002.

[4] Georgi Kalitzin and Gianluca Iaccarino, “Toward immersed boundary simulation of high

Reynolds number flows” , Center for Turbulence Research Annual Research Briefs 2003.

[5] Spalart, P. R. and Allmaras, S. R., “A one-equation tubulence model for aerdynamic flows,” La Recherche Aerospatiale, 1994, Vol. 1, 1-23.

[6] F. Tessicini y, G. Iaccarino, M. Fatica, M. Wang AND R. Verzicco, “Wall modeling for large-eddy simulation using an immersed boundary method”, Center for Turbulence Research Annual Research Briefs 2002.

[7] Sven Eisenbach and Rainer Friedrich, “Large-eddy simulation of flow separation on an airfoil at a high angle of attack and $Re = 10^5$ using Cartesian grids”,Theoretical and Computational Fluid Dynamics, Volme 22, Numbers 3-4/May, 2008, 213-225, 10.1007/s00162-007-0072-z.

[8] E.A. Fadlun, R. Verzicco, P. Orlandi, J. Mohd-Yusof, “Combined immersed-boundary/finite-difference methods for three-dimensional complex flow simulations”, J. Comput. Phys. 161 (2000) 35-60.

[9] M. Uhlmann, “An immersed boundary method with direct forcing for the simulation of particulate flows”, J. Comput. Phys. 184 (2003) 1-36.

[10] F.R. Menter, “Two-equation eddy-viscosity turbulence models for engineering applications”, AIAA J. 32(8) (1994) 1598-1605.

[11] A. Krzysiak, J. Narkiewicz, “Aerodynamic loads on airfoil with trailing-edge flap pitching with different frequencies”, Journal of Aircraft, 43(2) (2006) 407-418.